ACS Catalysis

Article

Identification of an Active NiCu Catalyst for Nitrile Synthesis from Alcohol

Yunzhu Wang, Shinya Furukawa, and Ning Yan

ACS Catal., **Just Accepted Manuscript** • DOI: 10.1021/acscatal.9b00043 • Publication Date (Web): 17 Jun 2019

Identification of an Active NiCu Catalyst for Nitrile Synthesis from Alcohol

Yunzhu Wang[†], *Shinya Furukawa**[‡§], *and Ning Yan**[†]

[†] Department of Chemical and Biomolecular Engineering, National University of Singapore, 4 Engineering Drive 4, Singapore 117585, Singapore.

[‡] Institute for Catalysis, Hokkaido University, N-21, W-10, Sapporo 001-0021, Japan.

[§] Elementary Strategy Initiative for Catalysis and Battery, Kyoto University, Kyoto Daigaku Katsura, Nishikyo-ku, Kyoto, Japan, 615-8510.

ABSTRACT: Development of heterogeneous catalysts for alcohol transformation into nitriles under oxidant free conditions is a challenge. Considering the C–H activation on α-carbon of primary alcohols is the rate-determining step, decreasing the activation energy of C–H activation is critical to enhance the catalytic activity. Several NiM/Al_2O_3 bimetallic

catalysts were synthesized and scrutinized in catalytic transformation of 1-butanol to butyronitrile. Ni–Cu was identified as a suitable combination with the optimized $Ni_{0.5}Cu_{0.5}/Al_2O_3$ catalyst exhibiting 10 times higher turnover frequency than Ni/Al_2O_3 catalyst. X-ray absorption spectroscopy (XAS) and high angle annular dark field scanning transmission electron microscopy (HAADF-STEM) revealed that the NiCu particles in the catalyst exist in the form of homogeneous alloys with an average size of 8.3 nm, providing experimental foundation to build up a catalyst model for further density functional theory (DFT) calculations. Calculations were done over a series of NiM catalysts, and the experimentally observed activity trend could be rationalized by the Brønsted–Evans–Polanyi (BEP) principle, i.e., catalysts afford reduced reaction energy also feature lower activation barriers. The calculated activation energy (E_a) for C–H activation with co-adsorbed NH_3 dropped from 63.4 kJ/mol on pure Ni catalyst to 49.9 kJ/mol on the most active NiCu-2 site in NiCu bimetallic catalyst, in good agreement with the experimentally measured activation energy values. The $Ni_{0.5}Cu_{0.5}/Al_2O_3$ catalyst was further employed to convert 11 primary alcohols into nitriles with high to near quantitative yields, at a Ni loading ten times less than the conventional Ni/Al_2O_3 catalyst.

Keywords: alcohol, nitrile, ammonia, BEP, heterogeneous catalyst, NiCu

1. INTRODUCTION

Nitriles are widely used to manufacture fine chemicals, pharmaceuticals, agrochemicals and polymers. Despite the commercial significance of nitriles, their traditional preparation methods, including Sandmeyer reaction[1], Rosenmund-von Braun reaction,[2] and the nucleophilic substitution of cyanides to alkyl and aryl halides,[3] generally require toxic starting materials and harsh reaction conditions.[4-8] In addition, stoichiometric amount of chemical wastes are often produced. Primary alcohols represent a class of alternative, greener starting material,[9-10] which can be converted to nitriles through oxygen-involved ammoxidation[11-20] or amination-dehydrogenation[21-26] reactions generating only H_2O and H_2 as by-products. Limited selectivity due to over-oxidation and/or high energy consumption associated with high reaction temperatures (280-500 °C) are the significant disadvantages in the current transformation of alcohols to nitriles using heterogeneous catalysts. In addition, despite the fact that various aromatic alcohols have been converted into corresponding nitriles on supported catalysts, transformation of aliphatic alcohols has been less successful.[13, 18, 20, 26-27]

Ni-based catalysts[28-38] have been extensively investigated in the hydrogen-free conversion of alcohols to primary amines, based on a “hydrogen-borrowing” strategy.[39-42] In this case, the amination reaction follows a dehydrogenation-imination-hydrogenation pathway, where alcohols are dehydrogenated to aldehydes/ketones and then react with ammonia to afford imines and finally to amines via hydrogenation. Recently, a Ni/Al_2O_3 catalyst was reported that converts a series of aliphatic and aromatic primary alcohols to nitriles under oxidant-free conditions.[43] The reaction followed a three-step dehydrogenation-imination-dehydrogenation pathway, similar to the amination reaction in the first two steps. Kinetics study revealed that C–H bond cleavage at α-carbon was the rate-determining step. A high amount of Ni (40 mg Ni per 1μ/min substrate) catalyst was used to achieve satisfactory yields of nitriles, and the nitrile selectivity for some substrates was below 90%. To further increase the catalytic performance, an improved catalyst to reduce the reaction barrier of the rate-determining step is essential.

Due to the unique electronic and geometric characteristics in the alloy or core-shell structure, bimetallic catalysts often show better catalytic performance than their single-component metal catalysts.[44] With its high tunability to form various bimetallic systems,

Ni is commonly employed as a base metal to construct bimetallic catalysts.[45-52] Of particular significance is the combination of Ni with other 3-d metal elements to form noble metal free bimetallic catalyst that are affordable and easily scalable. These catalysts have been used in a wide range of applications, and the superior catalytic activity has often been correlated to improved morphologies, electronic state and surface properties.[44] To our knowledge, however, bimetallic Ni based catalyst has not yet been systematically studied in alcohol transformation into amine and nitriles.

Recently, density functional theory (DFT) calculations become increasingly important to rationalize the performance of catalysts and to help catalyst design. Several groups have utilized a scaling relationship for catalysis research,[53-57] for example, to identify improved catalysts for propane dehydrogenation[55] and for ammonia synthesis.[57] Considering a major task of rational catalyst design is to reduce the reaction barrier, it is critical to predict the activation energy of a catalyst of given structure with reasonable accuracy. In physical chemistry, the BEP principle correlates the activation energies to the reaction energies of a series of reactions in a family with a linear relationship.[58-59] This empirical model helps predict the kinetic property (activation energy) of a reaction with its

thermodynamic property (reaction enthalpy). Applied in catalysis, DFT methods were generally used to demonstrate the BEP correlation of a surface-catalyzed elementary step. Many efforts have been devoted to reveal this correlation for molecule dissociation over transition-metal surfaces by varying the nature of the catalyst.[60-63] Bimetallic alloys differ from their parent metals in surface composition and electronic property, thus affecting the adsorption energies of substrates and products, and consequently the reaction energy.

Herein, we prepared a series of five NiM bimetallic catalysts for the nitrile synthesis from alcohols. NiCu was identified as the best combination affording the highest product yield and selectivity. The NiCu/Al_2O_3 catalysts with varied metal ratio were prepared, fully characterized and extensively evaluated in alcohol conversion into nitriles. The DFT calculations explicitly suggested that NiCu-bimetallic catalyst affords one of the lowest reaction energies and activation energies all NiM catalysts, providing a rational understanding of why NiCu is superior to single component Ni and other bimetallic NiM catalysts. The optimized NiCu/Al_2O_3 catalyst was applied to transform more than 10 primary alcohols into nitriles with high to near quantitative yields.

2. EXPERIMENTAL

2.1 Catalysts preparation

γ-Al_2O_3 was prepared by calcination of boehmite (γ-AlOOH, supplied by SASOL) at 900 °C for 3 h. Ni/Al_2O_3, Cu/Al_2O_3 and Ni–M/Al_2O_3 catalysts (M = Fe, Co, Cu, and Zn) were prepared by deposition-precipitation (DP) method or wet-impregnation (WI) method with loading amount of 6 wt%. Metal precursors included $Ni(NO_3)_2{\cdot}6H_2O$ (99%, Wako), $Cu(NO_3)_2{\cdot}3H_2O$ (99%, Sigma Aldrich), $Co(NO_3)_2{\cdot}6H_2O$ (98%, Wako), $Zn(NO_3)_2{\cdot}6H_2O$ (99%, Kanto) and $Fe(NO_3)_3{\cdot}9H_2O$ (98%, Sigma Aldrich). For DP method, aqueous solution of urea was dropwise added to a vigorously stirred mixture of γ-Al_2O_3 and aqueous solution of the metal precursors in a glass beaker. The molar ratio of Ni and M (Ni–M/Al_2O_3) was set to 1. The mixture was sealed tightly with a plastic film and heated with stirring on a hot stirrer. The temperature of the mixture was kept at 70 °C for 10 h (Cu and Ni–Cu) or 90 °C for 5 h (Ni, Ni–Co, Ni–Fe, and Ni–Zn). Note that, for Cu-containing catalysts, the temperature must not exceed 70 °C because dehydration of the

precipitated $Cu(OH)_2$ occurs to form aggregated CuO, typically resulting in fatal lowering of dispersion. Molar ratio of urea and the total amount of metals was set as 36 (Cu, Ni–Cu, Ni–Zn and Ni–Fe) or 15 (Ni, Ni–Co). After deposition, the colourless supernatant was removed and the resulting solid was washed with deionize water three times, followed by drying under reduced pressure. The resulting powder was calcined at 500 °C for 1 h, and then reduced at 400 °C (Cu/Al_2O_3) or 600 °C (Ni/Al_2O_3 and $Ni–M/Al_2O_3$) under 50 ml/min H_2 flow for 1 h. For WI method, γ-Al_2O_3 was added into an aqueous solution of metal precursors followed by stirring for 2 h at room temperature and drying under a reduced pressure. The obtained powder was calcined and reduced in a similar fashion as used in DP method.

Unsupported Ni, Cu, and NiCu particles were obtained by a precipitation method. A diluted solution of sodium hydroxide (NaOH, ≥ 98.5%, Sigma Aldrich, 0.05 M) was slowly added into a $Ni(NO_3)_2$ solution, a $Cu(NO_3)_2$ solution, or a mixture of $Ni(NO_3)_2$ and $Cu(NO_3)_2$ solution with molar ratio 1:1. The obtained slurry was washed and filtered with DI water and the solid was dried in an oven at 70 °C. The dried sample was calcined at 400 °C for 3 h, and reduced at 600 °C under 40 ml/min H_2 flow for 1 h.

2.2 Catalyst characterization

XAS was conducted at the BL01B1 station in SPring-8, using a Si(111) double-crystal monochromator. Energy calibration was under taken by using Cu foil. The spectra were recorded at room temperature at Ni and Cu K-edges in a transmission mode. For static measurements, the pelletized sample was pre-reduced by H_2 at 600 °C for 0.5 h, followed by sealing into a plastic pack together with an ISO A500-HS oxygen absorber (Fe powder) under N_2 atmosphere. Details for XAS data processing, as well as for X-ray diffraction (XRD), X-ray fluorescence (XRF), HAADF-STEM, energy-dispersive X-ray spectroscopy (EDS) and diffuse reflectance infrared Fourier transform spectroscopy (DRIFTS) analysis are provided in the supporting information.

2.3 General procedure for catalytic reactions

Catalytic evaluation experiments were carried out in a stainless steel, fixed-bed tube reactor (SS316, length 0.3 m, diameter 3/8 inch or 9.5 mm). The reactor was heated by

a furnace (Yuanbang Furnace, max 1000 °C) and its temperature was measured by a temperature probe located close to catalyst bed. A temperature controller was used to control the temperature of middle part of the tube reactor, where the catalysts were supported by a sieve and quartz wool. A syringe pump (Harvard PHD 2000 Infusion) was used to control the flow rate of liquid substrates in a glass syringe (Hamilton 81620), and the liquid substrates were supplied from the top of the reactor. The flow rates of NH_3 and N_2 are controlled by gas flow meters before they were mixed to carry the substrate through the catalyst bed.

All the catalysts were *in-situ* reduced with H_2 (50 mL/min) at 600 °C for 0.5 h before experiments. The reactor was cooled down to the reaction temperature under H_2 flow after reduction and N_2 was switched on to purge the system and remove physically adsorbed H_2. After that, the substrate, NH_3 and N_2 were supplied to the reactor, while the products and unconverted substrate were detected online with GC-FID using an Agilent HP-5 capillary column and He as the carrier gas. The organic products were enriched by passing through ethanol kept at 0 °C before GC-MS analysis.

2.4 Density functional theory (DFT) calculations

Periodic DFT calculations were performed using the CASTEP code[64] with Vanderbilt-type ultrasoft pseudopotentials[65] and the revised version of Perdew−Burke−Ernzerhof exchange−correlation functional based on the generalized gradient approximation.[66] Other details could be referred to an earlier publication[67] and are also available in the supporting information.

3. RESULTS AND DISCUSSION

3.1 Experimental identification of NiCu as an improved catalyst for butyronitrile synthesis

We prepared a series of NiM (M = Fe, Co, Cu, and Zn) alloys and pure Ni nanoparticles supported on Al_2O_3 by DP method, with 6 wt% Ni loading and 1:1 Ni:M ratio. The metallic phase of each catalyst was determined by the XRD patterns (Figure S1), and details of the catalysts were summarized in Table S1. Catalytic transformation of 1-butanol to butyronitrile was selected as a model reaction to compare the activity of the catalysts.

Pure Ni catalyst provided 13% butyronitrile. The $Ni_{0.5}Co_{0.5}$ catalyst was slightly better than pure Ni (14% yield), while the $Ni_{0.5}Cu_{0.5}$ catalyst was substantially better, affording a butyronitrile yield of 47% (Figure 1a). On the other side, incorporating Fe and Zn into Ni displayed a negative effect: $Ni_{0.5}Fe_{0.5}$ and $Ni_{0.5}Zn_{0.5}$ catalysts afforded only 3.5% and 4.7% butyronitrile, respectively. The $Ni_{0.5}Co_{0.5}$ and $Ni_{0.5}Cu_{0.5}$ alloy particles supported on Al_2O_3 with the same Ni loading were further prepared by WI method. The activity order follows: $Ni_{0.5}Cu_{0.5}$ > $Ni_{0.5}Co_{0.5}$ > Ni, which is in agreement with activity trend for catalysts prepared by DP method (data shown in Figure S2). From above, we confirm that the incorporation of a second 3-D metal element into Ni has a significant effect in transformation of alcohols to nitriles. Combination of Ni with its two adjacent elements, i.e., Co and Cu, results in an enhanced catalytic activity, in particular in the case of NiCu. The DP method in general provide more active catalyst than the WI method with the same metal composition, probably due to the fact that the DP method normally enables more uniform distribution of metal nanoparticles on the support.[68]

Subsequently, various NiCu catalysts with different metal loading and alloy phase were prepared by DP method. Alloy phase and particle size were easily modified *via* altering

preparation conditions. $Ni_{0.2}Cu_{0.8}$ in Figure 1b was prepared with 20 wt% Ni, while all the others contained 6 wt% Ni. For comparison purpose, pure Cu catalyst was prepared by the same method with 6 wt% metal loading. As shown in Figure 1b, the alloy phase is a critical factor affecting activity. Incorporation of Cu to Ni significantly enhanced the catalytic activity compared to pure Ni catalyst, the butyronitrile yield increased with decreasing Cu ratio. As Cu ratio decreased from 0.8 to 0.55, the butyronitrile yield increased from 22% to 46%. However, further decreasing the ratio of Cu induced a reduced butyronitrile yield, with 39% over $Ni_{0.75}Cu_{0.25}$ catalyst. Pure Cu catalyst caused high level of side reactions to produce 1-butylamine (Table S2), and resulted in lower selectivity towards butyronitrile, which is unfavored in nitrile production. This is probably because of the significant difference in C-H (and/or N-H) activating ability between Ni and Cu (Ni >> Cu, as demonstrated later by DFT calculation). Dehydrogenation of imine to nitrile seems to require high C-H (N-H) activation ability, while hydrogenation of imine to amine is preferable thermodynamically and kinetically. Imine intermediate on Cu prefers to be amine rather than nitrile due to the insufficient C-H (N-H) activation ability. The

$Ni_{0.5}Cu_{0.5}/Al_2O_3$ and Ni/Al_2O_3 mentioned in Figure 1a, and Cu/Al_2O_3 mentioned in Figure 1b prepared with DP method were selected for further study.

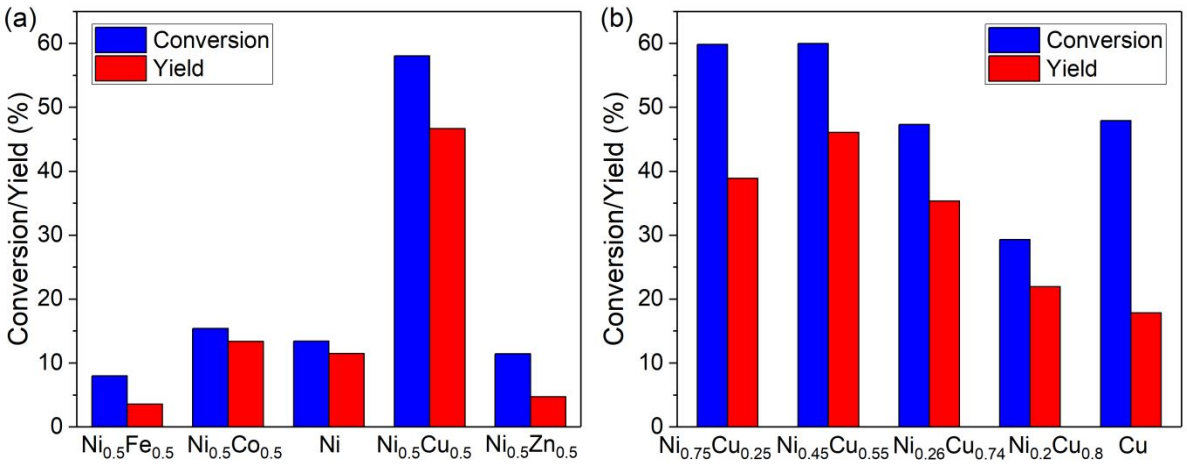

Figure 1. Catalytic activities of converting 1-butanol to butyronitrile with (a) various NiM/Al_2O_3 and Ni/Al_2O_3 catalysts prepared with DP method, and (b) various $NiCu/Al_2O_3$ and Cu/Al_2O_3 catalysts prepared with DP method. Reaction conditions: 1 μL/min 1-butanol, 8 mL/min NH_3, 20 mL/min N_2, 200 mg catalyst (or 60 mg $Ni_{0.2}Cu_{0.8}$), 160 °C, NH_3:1-butanol = 30:1.

3.2 Alloy structure of the NiCu catalyst

X-ray absorption near edge structure (XANES) spectra (Figure 2a-b) show that both Ni and Cu in $Ni_{0.5}Cu_{0.5}/Al_2O_3$ catalyst are close to the metallic states with a small amount of oxidized Ni species perhaps on the surface. $Ni_{0.5}Cu_{0.5}/Al_2O_3$ shows similar extended X-ray absorption fine structure (EXAFS) oscillations for Ni and Cu in the catalyst (Figure 2c). The periods are almost identical to each other for both Ni and Cu edges, and are intermediate between those of Ni foil and Cu foil. These are well consistent with the formation of 1:1 alloy confirmed by the XRD patterns (Figure S1). Fourier-transformed EXAFS (FT-EXAFS) spectra (Figure 2d-e) shows that only a small contribution of Ni–O bond to the spectrum of $Ni_{0.5}Cu_{0.5}/Al_2O_3$ is suggested, and Cu is almost in full metallic state. However, no feature of Ni–Ni shell of NiO was observed, indicating that the NiO_x species, if any, are insignificant. EXAFS curve fitting parameters are summarized in Table S3, and the M–M bond lengths of $Ni_{0.5}Cu_{0.5}/Al_2O_3$ for both edges were very close to the intermediate value (2.513 Å) of those for Ni foil (2.484 Å) and Cu foil (2.542 Å), which is also consistent with the formation of 1:1 alloy. No apparent difference in the coordination numbers was observed for Ni–Ni(Cu) and Cu–Cu(Ni) shells (9.1 and 8.8, respectively), supporting homogeneous alloying in the nanoparticles. The coordination number of Ni–O

shell in $Ni_{0.5}Cu_{0.5}/Al_2O_3$ was 1.1, indicating the existence of a small amount of Ni oxide species not participated in alloy formation.

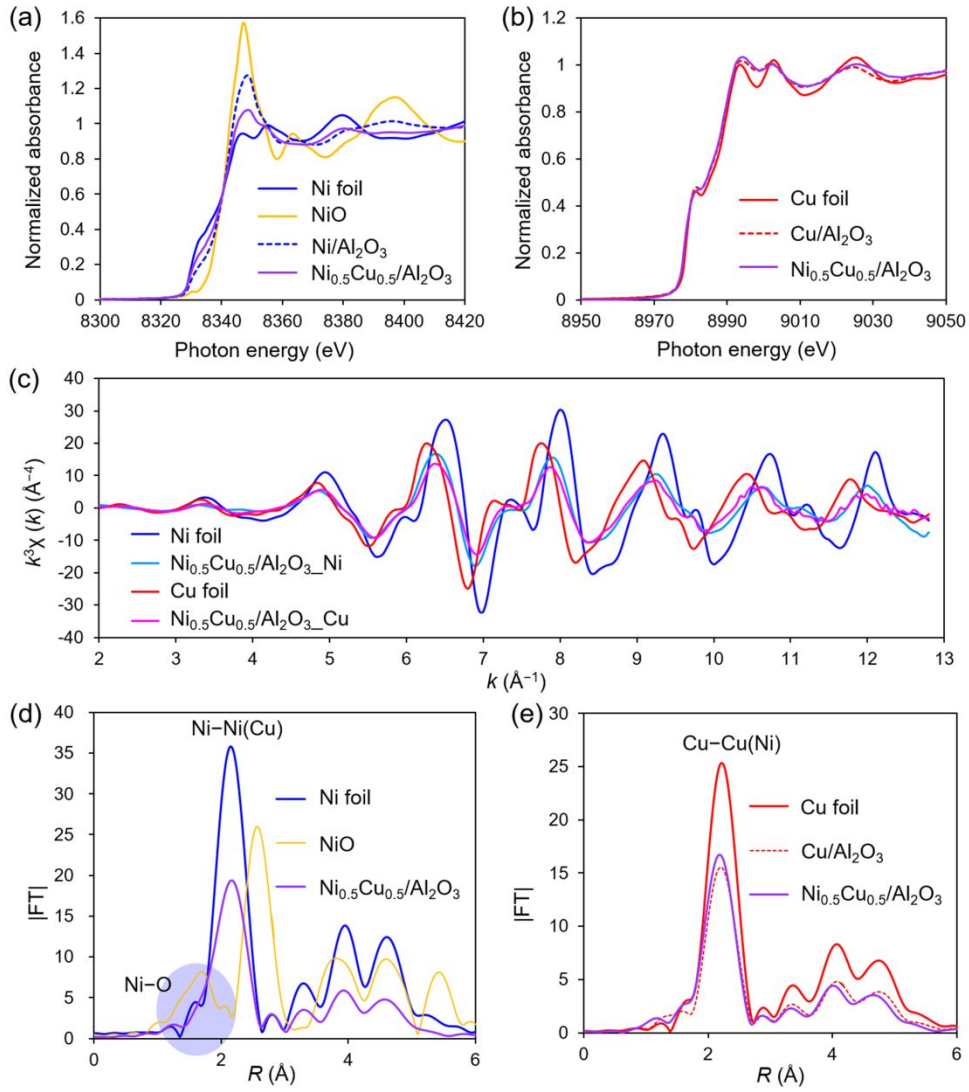

Figure 2. (a-b) XANES spectra, (c) EXAFS oscillations and (d-e) FT-EXAFS spectra of $Ni_{0.5}Cu_{0.5}/Al_2O_3$, Ni/Al_2O_3 and Cu/Al_2O_3 catalysts.

The STEM images of $Ni_{0.5}Cu_{0.5}/Al_2O_3$ show that nanoparticles are well dispersed, with an average particle size of 8.3 nm (Figure 3a-b). A high-resolution STEM image revealed that the nanoparticle had an fcc crystal structure (Figure 3c). EDS mapping images pronouncedly demonstrate that Ni and Cu are uniformly mixed (Figure 3d-f). These results strongly suggest that the nanoparticles are solid-solution alloy of Ni and Cu, which is consistent with the result of EXAFS. Surprisingly, Ni/Al_2O_3 and Cu/Al_2O_3 have much smaller particle sizes of 0.9 and 1.7 nm, respectively (Figure S3). According to idealized cubic close-packed full-shell metal clusters,[69-70] the surface atom percentage of the $Ni_{0.5}Cu_{0.5}/Al_2O_3$, Ni/Al_2O_3 and Cu/Al_2O_3 is estimated to be 17.1%, 87.3 % and 65.6% (Table S4), based on the average particle size.

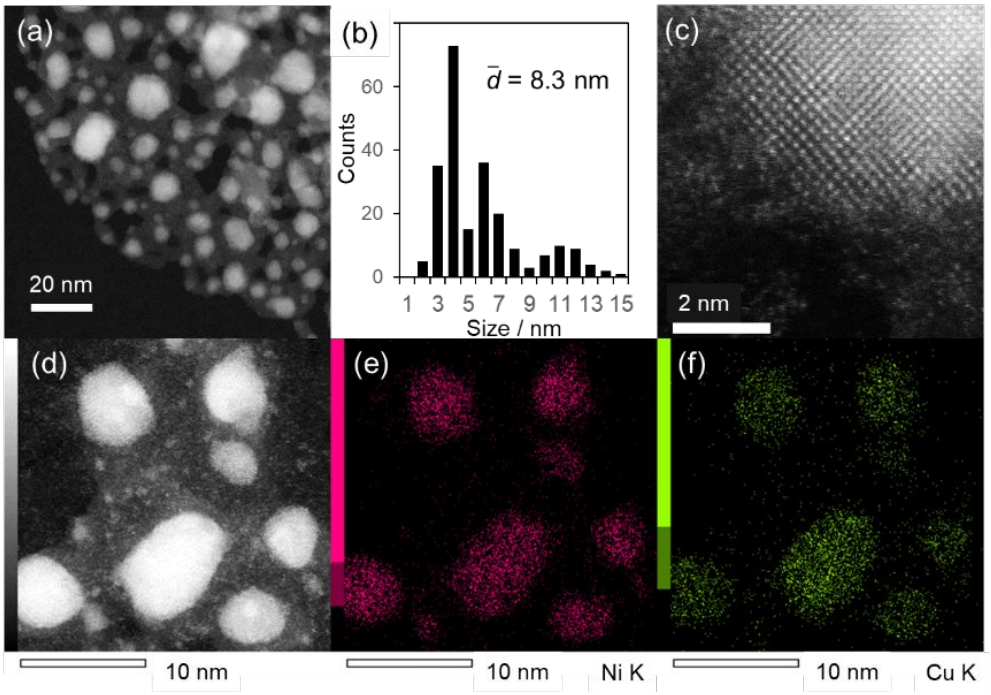

Figure 3. HAADF-STEM images of $Ni_{0.5}Cu_{0.5}/Al_2O_3$ and the corresponding elemental maps of Ni and Cu acquired by EDS: (a) STEM image, (b) size distribution, (c) high-resolution image of an fcc crystal viewed along [100] direction, (d) close-up of some nanoparticles, and element sensitive maps of (e) Ni and (f) Cu.

3.3 Reaction kinetics

Intrinsic activities of the three catalysts were measured when the conversions were kept low (< 30%). $Ni_{0.5}Cu_{0.5}/Al_2O_3$ afforded a high turnover frequency (TOF, measured by amount of butyronitrile produced per surface metal per hour) of 46 h^{-1}, an order of

magnitude higher than Ni/Al_2O_3 (4.9 h^{-1}) and Cu/Al_2O_3 (5.5 h^{-1}), as shown in Figure 4a. The conspicuously enhanced activity of $Ni_{0.5}Cu_{0.5}/Al_2O_3$ may be resulted from the lowered activation energy. Indeed, experimentally measured apparent E_a for $Ni_{0.5}Cu_{0.5}/Al_2O_3$ (51.6 kJ/mol) was much lower than Ni/Al_2O_3 (72.0 kJ/mol) and Cu/Al_2O_3 (78.2 kJ/mol) as shown in Figure 4b-d, which verifies our hypothesis.

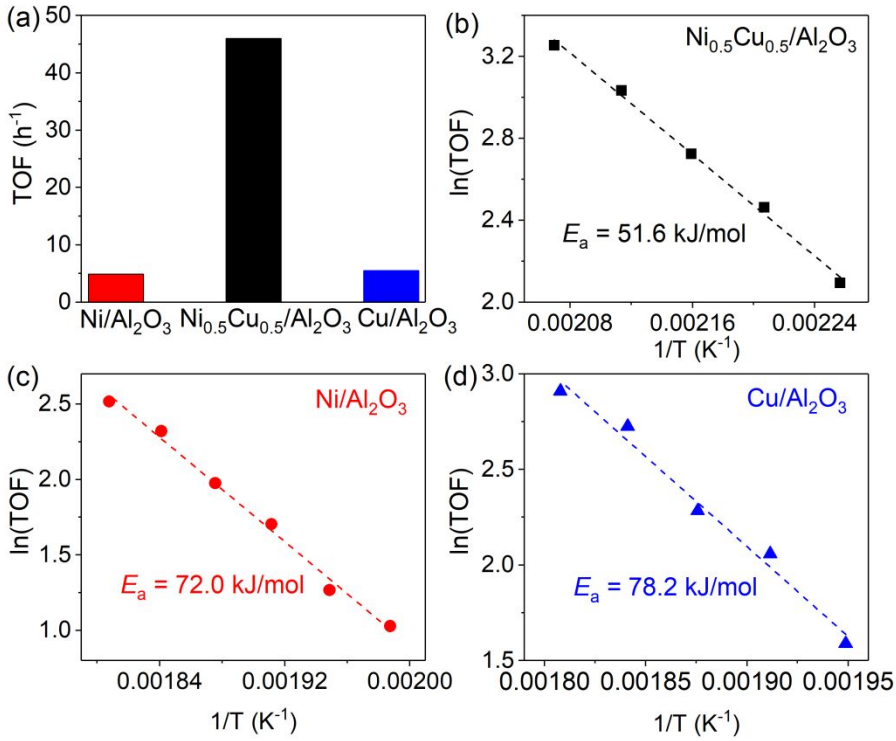

Figure 4. (a) TOFs towards production of butyronitrile at 210 °C. Reaction conditions: 4 ul/min 1-butanol, 8 ml/min NH_3, 92 ml/min N_2, 40 mg catalyst, 210 °C, NH_3:1-butanol = 7.5:1. (b-d) Activation energies of $Ni_{0.5}Cu_{0.5}/Al_2O_3$, Ni/Al_2O_3 and Cu/Al_2O_3 in the

conversion of 1-butanol to butyronitrile. Reaction conditions: 1 ul/min 1-butanol, 8 ml/min NH_3, 92 ml/min N_2, 10 mg catalyst, NH_3:1-butanol = 30:1.

The reaction orders of 1-butanol and NH_3 were measured at 210 ^oC to avoid thermodynamic limitation of the reaction. Since 1-butanol is easily vaporized under this condition, the reaction is regarded as two-phasic between gas and solid catalyst surface, and the reaction rate is assumed to follow the equation:

$$r = k * [1\text{-butanol}]^{\alpha} * [NH_3]^{\beta}$$

The reaction orders of 1-butanol and NH_3 were measured with constant concentration of the other reactant. As shown in Figure 5, NH_3 was adsorbed much stronger on the catalysts than 1-butanol resulting in negative orders, and competitive adsorption existed between NH_3 and 1-butanol. The positive order of 1-butanol indicated its activation may be involved in the rate determining step. The reaction order of alcohol increases from 0.63 to 0.83 after Cu incorporation, suggesting adsorption of 1-butanol on Ni was weakened in the NiCu alloy. On the other hand, incorporation of Cu to Ni did not change the NH_3 adsorption to an appreciable level (order of -0.14 to -0.13), which indicates that

NH_3 was probably adsorbed on Ni (or Ni rich) sites. For pure Cu catalyst, NH_3 adsorption afforded a close to 0 order (Figure S4), suggesting weaker adsorption of NH_3 than on Ni surface. After the kinetics study, we collected the spent $Ni_{0.5}Cu_{0.5}/Al_2O_3$ and Cu/Al_2O_3 catalysts for further characterizations. X-ray fluorescence (XRF) results (Table S5) revealed that the Ni and Cu contents in the spent catalyst were almost identical to those in the fresh catalyst, indicating that leaching of metal species was negligible. XRD patterns (Figure S5) confirmed the original 1:1 phase was retained in the $Ni_{0.5}Cu_{0.5}/Al_2O_3$ catalyst after reaction. The peak for $Ni_{0.5}Cu_{0.5}$ alloy did not become sharper, suggesting insignificant growth of the crystalline particle size.

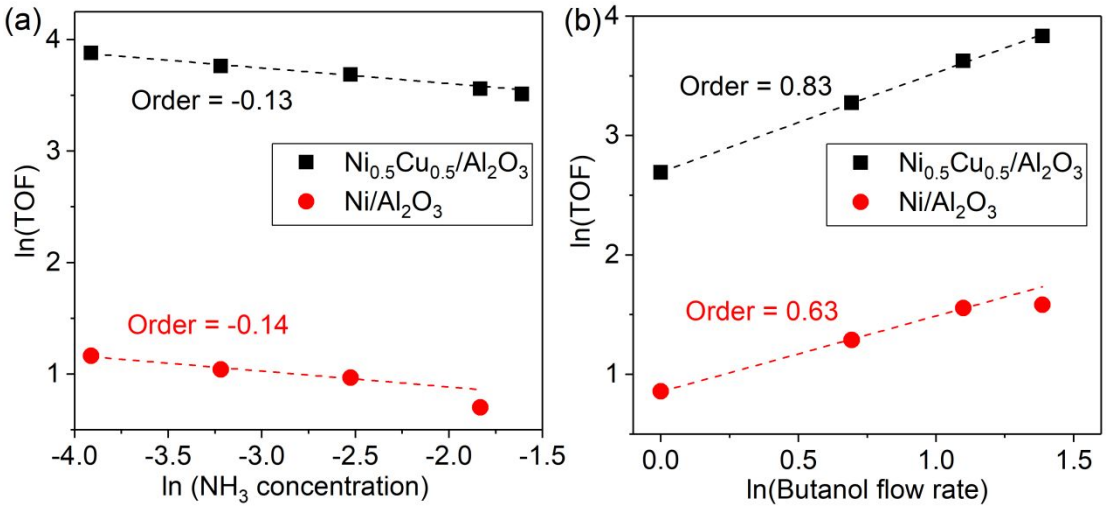

Figure 5. Plots of reaction orders for the conversion of 1-butanol to butyronitrile, of (a) NH_3, reaction conditions: 4 ul/min 1-butanol with 40 mg $Ni_{0.5}Cu_{0.5}/Al_2O_3$, or 3 ul/min 1-butanol with 80 mg Ni/Al_2O_3, 100 ml/min total gas flow rate with supplementing N_2, 210 °C; (b) 1-butanol, reaction conditions: 1 to 4 ul/min 1-butanol, 8 ml/min NH_3, 92 ml/min N_2, 40 mg $Ni_{0.5}Cu_{0.5}/Al_2O_3$ or 100 mg Ni/Al_2O_3, 210 °C.

Since product desorption and reactant adsorption may affect the reaction rate, the desorption rate of 1-butanol, butanal, 1-butylamine, and butyronitrile on metals were measured with *in-situ* DRIFTS. To avoid the effect of Al_2O_3, the DRIFTS analysis was measured on unsupported metal particles, which were prepared by co-deposition method and reduced under H_2 flow before measurement. The desorption behaviour was analysed at low temperature that no chemical reactions were observed. The desorption rates of the organic compounds are assumed to follow:

$$r_{des} = k_{des} * [\text{organic compound}]^{\gamma}$$

The adsorption spectra of the various compounds on NiCu, Ni, and Cu are shown in Figure S6-S8. The peak intensity of C–H stretching at around 2970 cm^{-1} was selected as an indicator of adsorbed amount, and the percentage of compounds which cannot be desorbed after stabilization was regarded as an indicator of adsorption strength. The desorption is assumed to follow first-order law, while the desorption rate constants were summarized in Table 1. R square numbers were also provided to highlight the fitting error. 1-butanol and butanal presented the slowest desorption rate constants on pure Ni, while incorporation of Cu increased their desorption rate constants, indicating their less stable adsorption on NiCu. This observation was consistent with the 1-butanol order obtained. In contrast, 1-butylamine had the slowest desorption rate constant on NiCu, and its stable adsorption on NiCu surface favoured further dehydrogenation to butyronitrile, promoting the reaction selectivity towards butyronitrile to some extent. Interestingly, the desorption of final product butyronitrile on three metal surfaces did not show much difference, indicating nitrile desorption is not the rate limiting step. In addition, close to 100% 1-butanol desorbed from NiCu surface under the applied temperature (Table S6), implying the weakened adsorption strength after Cu incorporation into Ni. In contrast, 82% 1-

butylamine remained on NiCu surface after stabilization for more than 30 mins, which was favourable as 1-butylamine could be further converted to butyronitrile. It is worth pointing out, however, that the values of all rate constants are within the same order of magnitude, suggesting the key differences of the catalysts do not lie in their ability to adsorb the starting material, or the product and side-product, or the aldehyde intermediate. On the other hand, the adsorption of 1-butanol on the surface of $Ni_{0.5}Cu_{0.5}/Al_2O_3$ catalyst was much slower, indicating the strong adsorption of 1-butanol or 1-butoxide on the real catalyst surface (Figure S9).

Table 1. Desorption rate constant based on first-order desorption rate[a]

Desorption Rate Constant (min^{-1})	NiCu	Ni	Cu
1-Butanol	0.38 (R^2 = 0.985)	0.27 (R^2 = 0.981)	0.47 (R^2 = 0.990)
Butanal	0.42 (R^2 = 0.969)	0.20 (R^2 = 0.874)	0.36 (R^2 = 0.948)
1-Butylamine	0.33 (R^2 = 0.974)	0.68 (R^2 = 0.987)	0.63 (R^2 = 0.963)

Butyronitrile	0.33 (R^2 = 0.970)	0.34 (R^2 = 0.989)	0.34 (R^2 = 0.990)

a. At t = 0, 10 μl of organic compounds were injected under N_2 flow, 130 °C.

Our previous work identified that the rate-determining step of the reaction is the C–H bond cleavage at α-carbon over pure Ni catalyst.[43] To verify whether this still applies on the NiCu bimetallic catalyst, a kinetic isotope effect (KIE) study was conducted using the $Ni_{0.5}Cu_{0.5}/Al_2O_3$ catalyst. 1-Butanol and isotope labelled substrate, 1-butanol-1,1-d_2 (deuteration of both H at the α-carbon of 1-butanol), was converted to butyronitrile at 160 °C. TOF obtained with $CH_3(CH_2)_2$–CD_2–OH was smaller than with 1-butanol, affording a KIE value of 1.89 (Table 2), which was slightly higher than that obtained over pure Ni catalyst in the previous work.[43] The modest positive value suggested that C–H bond breakage at α-carbon remain as a slow step in the overall reaction kinetics, establishing a starting point of the following DFT calculations.

Table 2. Kinetic isotopic effects for converting 1-butanol to butyronitrile

	Substrate	TOF (h^{-1})	KIE
1	1-butanol	5.94	
2	1-butanol-1,1-d_2	3.15	
3	$k_{1\text{-butanol}}$ / $k_{1\text{-butanol-1,1-d2}}$		1.89

Reaction conditions: 1 ul/min substrate, 2 ml/min NH_3, 23 ml/min N_2, 50 mg $Ni_{0.5}Cu_{0.5}/Al_2O_3$, 160 °C, NH_3:1-butanol = 7.5:1.

3.4 Energetics on the catalyst surface based on DFT

Based on the alloy structure revealed by XANES, EXAFS, XRD and STEM studies, we performed DFT calculations for the C–H activation of methoxide at various Ni-Cu hollow sites (Ni_3, Ni_2Cu, $NiCu_2$, and Cu_3, Figure 6a) with or without ammonia co-adsorbed, to better understand the energetics on the catalyst surface. Table 3 summarizes the adsorption (E_{ad}) and C–H activation energy of methoxide (E_a) and ΔE for various reaction sites of Ni and NiCu (entries 1~7). E_{ad} increased as the number of Cu atoms in the hollow

site (OMe site) increased, suggesting that Cu makes the adsorption of methoxide unfavorable. A good linear correlation was observed between E_{ad} and the number of Ni atoms included in the hollow site (0~3, Figure S10). Correction considering the contribution of Ni atoms in the second surface layer improved the linearity (R^2 = 0.993, Figure S10b). These results suggest that the adsorption strength depends dominantly on the surface atomic arrangement, but little on the bulk structure. E_a also varied widely depending on the Ni–Cu combination of the reaction site (Table 3). C–H cleavage occurring at Cu atom (conformation NiCu-4 and -6, entries 5 and 7, respectively) gave high E_a and ΔE, which reflects that Cu itself is less active for C–H activation of methoxide than Ni. The conformation NiCu-2, where the reaction occurs over Ni_2Cu hollow site, showed lower E_a and ΔE values than pure Ni (entries 1 and 3). The energetics of C–H activation in the presence of co-adsorbed ammonia was also studied, which is closer to the real situation. We focused on the effect of ammonia on the adsorption strength of methoxide and formaldehyde. A strong correlation was observed between the adjacency of the oxygen atom of formaldehyde and ammonia's hydrogen: E_{ad} became more negative as the O–H distance decreased (3.1 → 1.9 Å, Figure S11). This result strongly

suggests the formation of hydrogen bond (HB) between the carbonyl oxygen and ammonia's hydrogen, which stabilizes the adsorbates. On the contrary, for methoxide, E_{ad} was almost constant and independent on the distance to NH_3. This is probably because the oxygen atom of methoxide has already been fully coordinated (3 Ni and 1 C), hence the close contact of NH_3 is hindered sterically and electronically. Consequently, aldehyde is preferentially stabilized in the presence of NH_3, which significantly decreases ΔE. This trend was more prominent when the number of hydrogen bonding increased, while there was no effect when NH_3 was too far from the carbonyl oxygen (Figure S11 and Table 3 entries 10~12). The positive effect of NH_3 was also observed for the C–H activation at Cu sites (NiCu-4~NiCu-6: Table 3 entries 13~15). Thus, the co-adsorption of ammonia facilitates the C–H activation of methoxide kinetically and thermodynamically with the aid of hydrogen bonding. It should be noted that the calculated E_a for Ni (63.4 kJ/mol) and the most active NiCu-2 (49.9 kJ/mol) with ammonia are consistent with the corresponding experimental values obtained in this study (Ni: 72.0 kJ/mol, NiCu: 51.6 kJ/mol), hinting at the validity of DFT calculation. Figure 6b shows the plot of all the calculated E_a and ΔE, where a strong linear correlation was observed. This clearly

indicates that the C–H activation of alkoxide strongly follows the BEP relationship and that the catalytic activity (E_a) depends on the relative stability of the initial and final states (IS and FS, respectively). The alloying with Cu makes the alkoxide adsorption unfavored, thus providing more active sites with lower ΔE. Because less active sites with higher ΔE are also formed on the alloy surface, reaction site such as NiCu-2 would work as a true active site and contribute to the overall enhanced catalytic activity. In the presence of co-adsorbed ammonia, the FS (aldehyde) is stabilized by hydrogen bonding between the carbonyl oxygen and ammonia's hydrogen, thus further decreasing ΔE. Although there are two different factors to determine ΔE, i.e., the character of adsorption site and hydrogen bonding, the resulting ΔE can be a sole descriptor to determine E_a as represented by a strong linear BEP relationship.

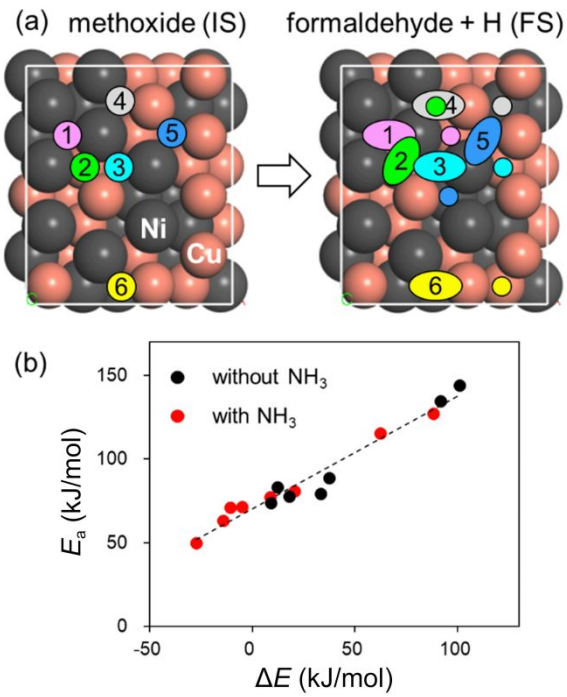

Figure 6. (a) Adsorption conformation of methoxide and formaldehyde + H on $Ni_{0.5}Cu_{0.5}$(111) alloy surface. Several conformations are numbered as NiCu-*n*. (b) Relationship between the calculated E_a and ΔE for Ni and NiCu in the absence and presence of ammonia.

Table 3. E_{ad}, E_a and ΔE in C–H activation of methoxide to formaldehyde at various sites of Ni and NiCu[a]

entry	conformation	Energy (kJ/mol)			OMe site	H site	C–H scission	N_{NH_3}	N_{HB}	R_{O-H} / Å [b]
		E_{ad}	E_a	ΔE						
1	Ni	-246.7	83.3	12.2	Ni_3	Ni_3	Ni	0	–	–
2	NiCu-1	-237.7	77.6	18.0	Ni_3	Ni_2Cu	Ni	0	–	–

3	**NiCu-2**	**-216.5**	**74.0**	**9.0**	**Ni_2Cu**	**Ni_2Cu**	**Ni**	0	–	–
4	NiCu-3	-219.3	79.5	33.4	Ni_2Cu	$NiCu_2$	Ni	0	–	–
5	NiCu-4	-222.2	144.4	100.7	Ni_2Cu	Cu_3	Cu	0	–	–
6	NiCu-5	-209.0	88.8	37.5	$NiCu_2$	Ni_2Cu	Ni	0	–	–
7	NiCu-6	-220.8	134.9	91.6	Ni_2Cu	Cu_3	Cu	0	–	–
8	Ni	-206.4	63.4	-14.2	Ni_3	Ni_3	Ni	3	1	2.48
9	Ni	-219.3	71.5	-5.1	Ni_3	Ni_3	Ni	2	1	3.12
10	**NiCu-2**	**-213.9**	**49.9**	**-27.3**	**Ni_2Cu**	**Ni_2Cu**	**Ni**	**3**	**2**	**1.89 (1.95)**
11	NiCu-2	-192.7	71.1	-10.7	Ni_2Cu	Ni_2Cu	Ni	3	1	2.05
12	NiCu-2	-219.2	77.3	8.8	Ni_2Cu	Ni_2Cu	Ni	2	0	4.17
13	NiCu-4	-186.5	127.5	88.1	Ni_2Cu	Cu_3	Cu	3	2	2.23 (2.54)
14	NiCu-5	-192.6	80.8	20.6	$NiCu_2$	Ni_2Cu	Ni	3	2	1.91 (2.27)
15	NiCu-6	-186.2	115.7	62.4	Ni_2Cu	Cu_3	Cu	3	2	1.94 (2.28)

a. N_{NH_3}: the number of ammonia molecules on the slab model, N_{HB}: the number of hydrogen bond between carbonyl oxygen and ammonia's hydrogen, R_{O-H}: distance between carbonyl oxygen and ammonia's hydrogen. Values in parentheses indicate the second closest distance.

We also considered the effect of ammonia on the electronic state of the metal surface. It is known that the position of the d-band center plays a key role to determine the adsorption strength of adsorbates: generally, the lower the d-band center is, the weaker the adsorption is.[71-73] We modeled a Ni(111) surface fully covered with ammonia and compared the d-band structures with and without ammonia. The density of states diagram projected on d orbital of the surface Ni atoms is shown in Figure S12. An intense band appeared at -1.5 eV shifted to -1.8 eV upon the full coverage of ammonia, which contributed to the downshift of d-band center (–1.46 to –1.86 eV). Therefore, on the basis

of the d band theory, adsorption on the Ni surface becomes weaker in the presence of ammonia. Indeed, E_{ad} of methoxide becomes less negative on each adsorption configuration (Table 3, entries 1→8, 3→10, 5→13, 6→14, and 7→15). Here, one should note that this might be a general trend just depending on surface coverage, hence not be specific for ammonia. Nevertheless, what is important is that the decrease in ΔE in the presence of ammonia cannot be explained by the electronic effect. This is because the electronic effect contributes to the decrease in E_{ad} not only of the reactant (methoxide), but also of the product (formaldehyde and hydrogen); therefore, ΔE would not change.

We extended the BEP theory to Ni and the NiM (M = Fe, Co, Cu, and Zn) series tested in this study, considering Ni(111) surface, NiM(111) (M = Fe, Co, and Cu) surfaces with NiM-2 configuration and intermetallic NiZn(101) surface (see Figures S13 and S14~17 for the detailed conformation and pictures of initial, transition, and final states). Figure 7a depicts the corresponding Ea–ΔE relationship with (2 hydrogen bond, notated as 2HB) and without ammonia adsorption (see Figure S18 and Table S7 for the energy profiles and the list of values, respectively). A good linear correlation was observed,

demonstrating that the BEP theory on the C–H activation process is generalizable for Ni-based alloys. We also evaluated the experimental catalytic activity of Ni/Al_2O_3 and NiM/Al_2O_3 on the basis of *Ea*. Figure 7b represents the log of the measured reaction rate plotted against calculated *Ea*, which showed a negative linear correlation. This correlation is well consistent with the Arrhenius equation and indicates that the catalytic activity is governed by the energetics of alkoxide activation. Thus, the calculations well explained the observed experimental trend.

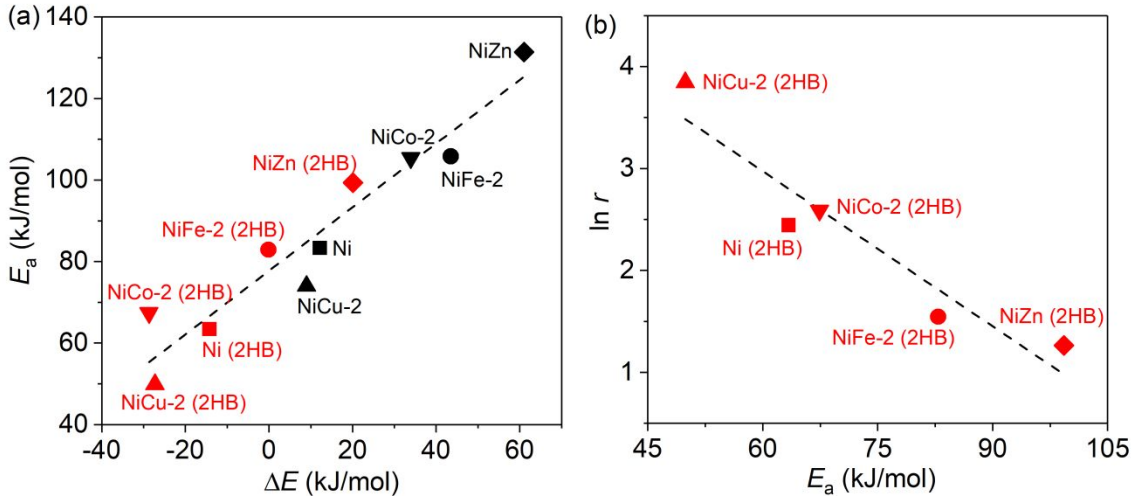

Figure 7. Correlations between (a) E_a and Δ*E* and (b) ln *r* (*r*: reaction rate = formation rate of nitrile) and E_a of C–H activation from methoxide to formaldehyde over Ni(111), NiM(111) (M = Fe, Co, and Cu) surfaces with NiM-2 configuration and intermetallic NiZn(101) surface. For (a), the plot was made among surfaces with ammonia co-adsorbed (red color)

and without ammonia co-adsorbed (black color). For (b), the plot was made among surfaces with ammonia co-adsorbed.

3.5 Substrate scope

We finally inspect the applicability of optimized catalyst to make other nitriles. 11 primary alcohols have been used as substrate to react with NH_3 over the $Ni_{0.5}Cu_{0.5}/Al_2O_3$ catalyst. The catalytic system was active in transforming aliphatic alcohols, affording nitrile in 63%-95% yields (Table 4). Slightly lower activities were observed towards transforming alcohols bearing aromatic rings, with nitriles yields varied from 52% to 81% with doubled catalyst loading. Notably, high selectivity (91% to 99%) towards nitriles were always obtained with both aliphatic and aromatic alcohols, suggesting the $Ni_{0.5}Cu_{0.5}/Al_2O_3$ catalyst to be task-specific, and that facile separation and purification of the product can be achieved. Compared with previous reported pure Ni catalyst,[43] more than 90% less Ni is needed to achieve the same level of yield under the same condition.

Table 4. $Ni_{0.5}Cu_{0.5}/Al_2O_3$ catalyzed conversion of various alcohols to corresponding nitriles

$$R\text{-}CH_2\text{-}OH + NH_3 \xrightarrow[\triangle]{Ni_{0.5}Cu_{0.5}/Al_2O_3} R\text{-}CN + 2H_2 + H_2O$$

Entry	Substrate	Product	Yield (%)	Selectivity (%)
1	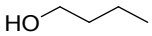	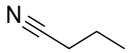	94	97
2	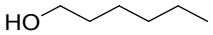	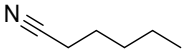	84	99
3	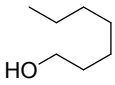	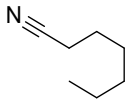	95	98
4	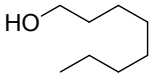	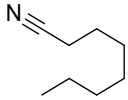	92	98
5	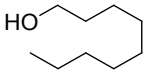	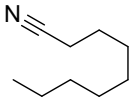	63	90
6	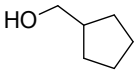	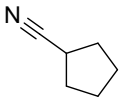	82	96
7	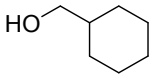	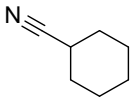	88	90
8[a]	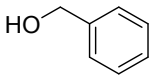	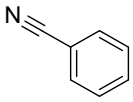	90	90
9[a]	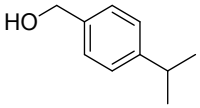	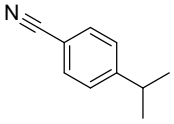	67	93
10[a]	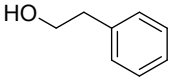	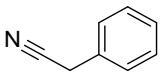	60	92

11[a]	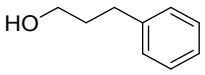	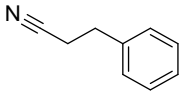	81	95

Reaction conditions: 1 μL/min substrate, 2 mL/min NH_3, 23 mL/min N_2, 50 mg $Ni_{0.5}Cu_{0.5}/Al_2O_3$, 240 °C.

a. 100 mg catalyst.

4. CONCLUSION

The C–H bond cleavage at the α-carbon is regarded as the rate limiting step in nitrile formation from alcohols. To enhance the catalytic activity by facilitating the rate-determining step, a series of NiM/Al_2O_3 catalysts was synthesized with varied preparation methods and structures. Among these, a $Ni_{0.5}Cu_{0.5}/Al_2O_3$ catalyst with a homogeneous alloy structure and particle size at around 8 nm presented 10 times higher TOF than reported pure Ni/Al_2O_3 catalyst in the reaction of 1-butanol to butyronitrile. The apparent activation energy decreases from 72.0 kJ/mol for the Ni/Al_2O_3 catalyst to 51.6 kJ/mol for the $Ni_{0.5}Cu_{0.5}/Al_2O_3$ catalyst. The optimized NiCu catalyst was also applied to convert 11 primary alcohols with Ni loading 10 times less than using pure Ni catalyst to achieve the same level of yields.

Based on DFT calculations, NH_3 was found to reduce the reaction energies over all the NiM catalysts and make the C–H activation thermodynamically favourable, plausibly due to the hydrogen bonding preferentially stabilizing the FS. The calculations rationalized NiCu as a better catalyst for the reaction, since it possesses lower reaction energies than pure Ni, and thus lowers reaction barriers following the BEP principle. The calculated reaction barrier of C–H activation were fully consistent with the experimental data for the activation energies. Considering C–H activation is also the rate-limiting step of several other important reactions such as alcohol oxidation as well as alcohols to amines, this approach for catalyst identification and rationalization may be generalizable in designing improved catalysts for more applications.

AUTHOR INFORMATION

Corresponding Author

*E-mail: ning.yan@nus.edu.sg

*E-mail: furukawa@cat.hokudai.ac.jp

ORCID

Yunzhu Wang: 0000-0001-5315-0174

Shinya Furukawa: 0000-0002-2621-6139

Ning Yan: 0000-0002-1877-9206

Notes

The authors declare no competing financial interest

ASSOCIATED CONTENT

Supporting Information

The Supporting Information is available free of charge on the ACS Publications website at DOI:

Experimental procedures and supplementary figures (PDF)

ACKNOWLEDGMENTS

This work was supported by the National University of Singapore and Ministry of Education, Singapore (R-279-000-462-112 and R-279-000-464-133) and by JSPS KAKENHI (Grant Number 17H04965). Computation time was provided by the SuperComputer System, Institute for Chemical Research, Kyoto University.

REFERENCES

(1) Galli, C. Radical Reactions of Arenediazonium Ions: An Easy Entry into the Chemistry of the Aryl Radical. *Chem. Rev.* **1988,** *88*, 765-792.

(2) Lindley, J. Tetrahedron Report Number 163: Copper Assisted Nucleophilic Substitution of Aryl Halogen. *Tetrahedron* **1984,** *40*, 1433-1456.

(3) Anbarasan, P.; Schareina, T.; Beller, M. Recent Developments and Perspectives in Palladium-Catalyzed Cyanation of Aryl Halides: Synthesis of Benzonitriles. *Chem. Soc. Rev.* **2011,** *40*, 5049-5067.

(4) Sundermeier, M.; Mutyala, S.; Zapf, A.; Spannenberg, A.; Beller, M. A Convenient and Efficient Procedure for the Palladium-Catalyzed Cyanation of Aryl Halides using Trimethylsilylcyanide. *J. Organomet. Chem.* **2003,** *684*, 50-55.

(5) Zanon, J.; Klapars, A.; Buchwald, S. L. Copper-Catalyzed Domino Halide Exchange-Cyanation of Aryl Bromides. *J. Am. Chem. Soc.* **2003,** *125*, 2890-2891.

(6) Cristau, H.-J.; Ouali, A.; Spindler, J.-F.; Taillefer, M. Mild and Efficient Copper-Catalyzed Cyanation of Aryl Iodides and Bromides. *Chem. Eur. J.* **2005,** *11*, 2483-2492.

(7) Schareina, T.; Zapf, A.; Mägerlein, W.; Müller, N.; Beller, M. A New Palladium Catalyst System for the Cyanation of Aryl Chlorides with $K_4[Fe(CN)_6]$. *Tetrahedron Lett.* **2007,** *48*, 1087-1090.

(8) Buono, F. G.; Chidambaram, R.; Mueller, R. H.; Waltermire, R. E. Insights into Palladium-Catalyzed Cyanation of Bromobenzene: Additive Effects on the Rate-Limiting Step. *Org. Lett.* **2008,** *10*, 5325-5328.

(9) Beltram, A.; Melchionna, M.; Montini, T.; Nasi, L.; Fornasiero, P.; Prato, M. Making H_2 from Light and Biomass-Derived Alcohols: the Outstanding Activity of newly Designed Hierarchical MWCNT/Pd@TiO_2 Hybrid Catalysts. *Green Chem.* **2017,** *19*, 2379-2389.

(10) Foo, G. S.; Hood, Z. D.; Wu, Z. Shape Effect Undermined by Surface Reconstruction: Ethanol Dehydrogenation over Shape-Controlled $SrTiO_3$ Nanocrystals. *ACS Catal.* **2018,** *8*, 555-565.

(11) Oishi, T.; Yamaguchi, K.; Mizuno, N. Catalytic Oxidative Synthesis of Nitriles Directly from Primary Alcohols and Ammonia. *Angew. Chem. Int. Ed.* **2009,** *48*, 6286-6288.

(12) Martin, A.; Kalevaru, V. N. Heterogeneously Catalyzed Ammoxidation: A Valuable Tool for One-Step Synthesis of Nitriles. *ChemCatChem* **2010,** *2*, 1504-1522.

(13) Ishida, T.; Watanabe, H.; Takei, T.; Hamasaki, A.; Tokunaga, M.; Haruta, M. Metal Oxide-Catalyzed Ammoxidation of Alcohols to Nitriles and Promotion Effect of Gold Nanoparticles for One-Pot Amide Synthesis. *Appl. Catal., A* **2012,** *425-426*, 85-90.

(14) Dornan, L. M.; Cao, Q.; Flanagan, J. C.; Crawford, J. J.; Cook, M. J.; Muldoon, M. J. Copper/TEMPO Catalysed Synthesis of Nitriles from Aldehydes or Alcohols Using Aqueous Ammonia and with Air as the Oxidant. *Chem. Commun.* **2013,** *49*, 6030-6032.

(15) Yin, W.; Wang, C.; Huang, Y. Highly Practical Synthesis of Nitriles and Heterocycles from Alcohols under Mild Conditions by Aerobic Double Dehydrogenative Catalysis. *Org. Lett.* **2013,** *15*, 1850-1853.

(16) Yadav, D. K. T.; Bhanage, B. M. Copper-Catalyzed Synthesis of Nitriles by Aerobic Oxidative Reaction of Alcohols and Ammonium Formate. *Eur. J. Org. Chem.* **2013,** *2013*, 5106-5110.

(17) Xie, J.-B.; Bao, J.-J.; Li, H.-X.; Tan, D.-W.; Li, H.-Y.; Lang, J.-P. An Efficient Approach to the Ammoxidation of Alcohols to Nitriles and the Aerobic Oxidation of Alcohols to Aldehydes in Water Using Cu(II)/Pypzacac Complexes as Catalysts. *RSC Adv.* **2014,** *4*, 54007-54017.

(18) Jagadeesh, R. V.; Junge, H.; Beller, M. Green Synthesis of Nitriles Using Non-Noble Metal Oxides-Based Nanocatalysts. *Nat. Commun.* **2014,** *5*, 4123.

(19) Hamill, C.; Driss, H.; Goguet, A.; Burch, R.; Petrov, L.; Daous, M.; Rooney, D. Mild Temperature Palladium-Catalyzed Ammoxidation of Ethanol to Acetonitrile. *Appl. Catal., A* **2015,** *506*, 261-267.

(20) Shang, S.; Wang, L.; Dai, W.; Chen, B.; Lv, Y.; Gao, S. High Catalytic Activity of Mesoporous Co–N/C Catalysts for Aerobic Oxidative Synthesis of Nitriles. *Catal. Sci. Technol.* **2016,** *6*, 5746-5753.

(21) Bashkirov, A. N.; Zakirov, N. S.; Abdurakhmanov, E. A.; Kliger, G. A.; Muradov, K.; Snagovskii, Y. S. Optimization of the Process of Synthesis of Aliphatic Nitriles from Alcohols and Ammonia. *Neftekhimiya* **1987,** *27*, 818-821.

(22) Zhang, D.; Zhang, Y.; Wen, Y.; Hou, K.; Zhao, J. Intrinsic Kinetics for the Synthesis of Acetonitrile from Ethanol and Ammonia over Co–Ni/γ–Al_2O_3 Catalyst. *Chem. Eng. Res. Des.* **2011,** *89*, 2147-2152.

(23) Zhang, Y.; Xu, W.; Zhao, J. Synthesis of Phenylacetonitrile by Amination of Styrene Oxide Catalyzed by a Bimetallic Catalyst $Zn_{30.1}Cr_{4.3}$/γ-Al_2O_3. *RSC Adv.* **2012,** *2*, 6590-6598.

(24) Zhang, Y.; Wei, T.; Pian, Y.; Zhao, J. Amination of Allyl Alcohol to Propionitrile over a $Zn_{30}Cr_{4.5}$/γ-Al_2O_3 Bimetallic Catalyst via Coupled Dehydrogenation–Hydrogenation Reactions. *Appl. Catal., A* **2013,** *467*, 154-162.

(25) Hu, Y.; Jin, S.; Zhang, Z.; Zhang, L.; Deng, J.; Zhang, H. One-Step Synthesis of Nitriles by the Dehydrogenation–Amination of Fatty Primary Alcohols over Cu/m-ZrO_2. *Catal. Commun.* **2014,** *54*, 45-49.

(26) Zhang, Y.; Zhao, X.; Zhang, H.; Yan, X.; Zhao, J. Conversion of Benzyl Alcohol to Benzonitrile over a $Cu_{10.3}$/SiO_2 Catalyst. *Appl. Catal., A* **2016,** *522*, 45-53.

(27) Shang, S.; Dai, W.; Wang, L.; Lv, Y.; Gao, S. Metal-free Catalysis of Nitrogen-Doped Nanocarbons for the Ammoxidation of Alcohols to Nitriles. *Chem Commun* **2017,** *53*, 1048-1051.

(28) Shimizu, K.-i.; Kon, K.; Onodera, W.; Yamazaki, H.; Kondo, J. N. Heterogeneous Ni Catalyst for Direct Synthesis of Primary Amines from Alcohols and Ammonia. *ACS Catal.* **2013,** *3*, 112-117.

(29) Shimizu, K.-i.; Kanno, S.; Kon, K.; Hakim Siddiki, S. M. A.; Tanaka, H.; Sakata, Y. N-Alkylation of Ammonia and Amines with Alcohols Catalyzed by Ni-loaded $CaSiO_3$. *Catal. Today* **2014,** *232*, 134-138.

(30) Liu, Y.; Zhou, K.; Shu, H.; Liu, H.; Lou, J.; Guo, D.; Wei, Z.; Li, X. Switchable Synthesis of Furfurylamine and TetrahydrofurFurylamine from Furfuryl Alcohol over RANEY® Nickel. *Catal. Sci. Technol.* **2017,** *7*, 4129-4135.

(31) Tomer, A.; Wyrwalski, F.; Przybylski, C.; Paul, J.-F.; Monflier, E.; Pera-Titus, M.; Ponchel, A. Facile Preparation of Ni/Al_2O_3 Catalytic Formulations with the Aid of Cyclodextrin Complexes: Towards Highly Active and Robust Catalysts for the Direct Amination of Alcohols. *J. Catal.* **2017,** *356*, 111-124.

(32) Tomer, A.; Yan, Z.; Ponchel, A.; Pera-Titus, M. Mixed Oxides Supported Low-Nickel Formulations for the Direct Amination of Aliphatic Alcohols with Ammonia. *J. Catal.* **2017,** *356*, 133-146.

(33) Wang, W.; Yu, Q.; Zhang, Q.; Mei, S.; Yuan, J.; Zhao, F.; Yang, J.; Lu, J. Reductive Amination of 2-Amino-2-methyl-1-propanol and Ammonia to Produce 2-Methyl-1,2-propanediamine over Raney Nickel Catalyst. *ChemistrySelect* **2017,** *2*, 8818-8823.

(34) Dumon, A. S.; Wang, T.; Ibañez, J.; Wischert, R.; Sautet, P.; Tomer, A.; Pera-Titus, M.; Yan, Z.; Michel, C. Direct n-Octanol Amination by Ammonia on Supported Ni and Pd Catalysts: Activity is Enhanced by "Spectator" Ammonia Adsorbates. *Catal. Sci. Technol.* **2018,** *8*, 611-621.

(35) Leung, A. Y. K.; Hellgardt, K.; Hii, K. K. M. Catalysis in Flow: Nickel-Catalyzed Synthesis of Primary Amines from Alcohols and NH_3. *ACS Sustainable Chem. Eng.* **2018,** *6*, 5479-5484.

(36) Ma, L.; Sun, K.; Luo, M.; Yan, L.; Jiang, Z.; Lu, A.-H.; Ding, Y. Role of ReO_x Species in Ni-Re/Al_2O_3 Catalyst for Amination of Monoethanolamine. *J. Phys. Chem. C* **2018,** *122*, 23011-23025.

(37) Ma, L.; Yan, L.; Lu, A.-H.; Ding, Y. Effect of Re Promoter on the Structure and Catalytic Performance of Ni–Re/Al_2O_3 Catalysts for the Reductive Amination of Monoethanolamine. *RSC Adv.* **2018,** *8*, 8152-8163.

(38) Tomer, A.; Kusema, B. T.; Paul, J.-F.; Przybylski, C.; Monflier, E.; Pera-Titus, M.; Ponchel, A. Cyclodextrin-Assisted Low-Metal Ni-Pd/Al_2O_3 Bimetallic Catalysts for the Direct Amination of Aliphatic Alcohols. *J. Catal.* **2018,** *368*, 172-189.

(39) Edwards, M. G.; Jazzar, R. F. R.; Paine, B. M.; Shermer, D. J.; Whittlesey, M. K.; Williams, J. M. J.; Edney, D. D. Borrowing Hydrogen: A Catalytic Route to C–C Bond Formation from Alcohols. *Chem. Commun.* **2004,** 90-91.

(40) Watson, A. J.; Williams, J. M. The Give and Take of Alcohol Activation. *Science* **2010,** *329*, 635-636.

(41) Gunanathan, C.; Milstein, D. Applications of Acceptorless Dehydrogenation and Related Transformations in Chemical Synthesis. *Science* **2013,** *341*, 1229712.

(42) Tamura, M.; Arai, T.; Nakagawa, Y.; Tomishige, K. Transformation of Diols to Ketones via Intramolecular Borrowing Hydrogen Mechanism. *Chem. Lett.* **2017,** *46*, 1333-1336.

(43) Wang, Y.; Furukawa, S.; Zhang, Z.; Torrente-Murciano, L.; Khan, S. A.; Yan, N. Oxidant Free Conversion of Alcohols to Nitriles over Ni-Based Catalysts. *Catal. Sci. Technol.* **2019,** *9*, 86-96.

(44) De, S.; Zhang, J.; Luque, R.; Yan, N. Ni-based Bimetallic Heterogeneous Catalysts for Energy and Environmental Applications. *Energy Environ. Sci.* **2016,** *9*, 3314-3347.

(45) Zhang, J.; Zhao, C. Development of a Bimetallic Pd-Ni/HZSM-5 Catalyst for the Tandem Limonene Dehydrogenation and Fatty Acid Deoxygenation to Alkanes and Arenes for Use as Biojet Fuel. *ACS Catal.* **2016,** *6*, 4512-4525.

(46) Ren, Z.; Wu, Z.; Song, W.; Xiao, W.; Guo, Y.; Ding, J.; Suib, S. L.; Gao, P.-X. Low Temperature Propane Oxidation over Co_3O_4 based Nano-Array Catalysts: Ni Dopant Effect, Reaction Mechanism and Structural Stability. *Appl. Catal., B* **2016,** *180*, 150-160.

(47) Luo, Z.; Zheng, Z.; Li, L.; Cui, Y.-T.; Zhao, C. Bimetallic Ru–Ni Catalyzed Aqueous-Phase Guaiacol Hydrogenolysis at Low H_2 Pressures. *ACS Catal.* **2017,** *7*, 8304-8313.

(48) Tomishige, K.; Li, D.; Tamura, M.; Nakagawa, Y. Nickel–Iron Alloy Catalysts for Reforming of Hydrocarbons: Preparation, Structure, and Catalytic Properties. *Catal. Sci. Technol.* **2017,** *7*, 3952-3979.

(49) Luo, J.; Monai, M.; Wang, C.; Lee, J. D.; Duchoñ, T.; Dvořák, F.; Matolí-n, V.; Murray, C. B.; Fornasiero, P.; Gorte, R. J. Unraveling the Surface State and Composition of Highly Selective Nanocrystalline Ni-Cu Alloy Catalysts for Hydrodeoxygenation of HMF. *Catal. Sci. Technol.* **2017,** *7*, 1735-1743.

(50) Goulas, K. A.; Lee, J. D.; Zheng, W.; Lym, J.; Yao, S.; Oh, D. S.; Wang, C.; Gorte, R. J.; Chen, J. G.; Murray, C. B.; Vlachos, D. G. Spectroscopic Characterization of A Highly Selective $NiCu_3$/C Hydrodeoxygenation Catalyst. *Catal. Sci. Technol.* **2018,** *8*, 6100-6108.

(51) Shen, X.; Zhang, C.; Zhang, S.; Dai, S.; Zhang, G.; Ge, M.; Pan, Y.; Sharkey, S. M.; Graham, G. W.; Hunt, A.; Waluyo, I.; Miller, J. T.; Pan, X.; Peng, Z. Deconvolution of Octahedral Pt_3Ni Nanoparticle Growth Pathway from in situ Characterizations. *Nat. Commun.* **2018,** *9*, 4485.

(52) Joshi, R.; Zhang, G.; Miller, J. T.; Gounder, R. Evidence for the Coordination–Insertion Mechanism of Ethene Dimerization at Nickel Cations Exchanged onto Beta Molecular Sieves. *ACS Catal.* **2018,** *8*, 11407-11422.

(53) Tamura, M.; Kon, K.; Satsuma, A.; Shimizu, K.-i. Volcano-Curves for Dehydrogenation of 2-Propanol and Hydrogenation of Nitrobenzene by SiO_2-Supported Metal Nanoparticles Catalysts As Described in Terms of a d-Band Model. *ACS Catal.* **2012,** *2*, 1904-1909.

(54) Lansford, J. L.; Mironenko, A. V.; Vlachos, D. G. Scaling Relationships and Theory for Vibrational Frequencies of Adsorbates on Transition Metal Surfaces. *Nat. Commun.* **2017,** *8*, 1842.

(55) Sun, G.; Zhao, Z. J.; Mu, R.; Zha, S.; Li, L.; Chen, S.; Zang, K.; Luo, J.; Li, Z.; Purdy, S. C.; Kropf, A. J.; Miller, J. T.; Zeng, L.; Gong, J. Breaking the Scaling Relationship *via* Thermally Stable Pt/Cu Single Atom Alloys for Catalytic Dehydrogenation. *Nat. Commun.* **2018,** *9*, 4454.

(56) Sandberg, R. B.; Hansen, M. H.; Abild-Pedersen, J. K. N. F.; Bajdich, M. Strongly Modified Scaling of CO Hydrogenation in Metal Supported TiO Nanostripes. *ACS Catal.* **2018,** *8*, 10555−10563.

(57) Singh, A. R.; Montoya, J. H.; Rohr, B. A.; Tsai, C.; Vojvodic, A.; Nørskov, J. K. Computational Design of Active Site Structures with Improved Transition-State Scaling for Ammonia Synthesis. *ACS Catal.* **2018,** *8*, 4017-4024.

(58) Brønsted, J. N. Acid and Basic Catalysis. *Chem. Rev.* **1928,** *5*, 231-338.

(59) Evans, M. G.; Polanyl, M. Inertia and Driving Force of Chemical Reactions. *Trans. Faraday Soc.* **1937,** *34*, 11-24.

(60) Nørskov, J. K.; Bligaard, T.; Logadottir, A.; Bahn, S.; Hansen, L. B.; Bollinger, M.; Bengaard, H.; Hammer, B.; Sljivancanin, Z.; Mavrikakis, M.; Xu, Y.; Dahl, S.; Jacobsen, C. J. H. Universality in Heterogeneous Catalysis. *J. Catal.* **2002,** *209*, 275-278.

(61) Loffreda, D.; Delbecq, F.; Vigne, F.; Sautet, P. Fast Prediction of Selectivity in Heterogeneous Catalysis from Extended Bronsted-Evans-Polanyi Relations: A Theoretical Insight. *Angew. Chem. Int. Ed.* **2009,** *48*, 8978-8980.

(62) Santen, R. A. v.; Neurock, M.; Shetty, S. G. Reactivity Theory of Transition-Metal Surfaces: A Brønsted-Evans-Polanyi Linear Activation Energy-Free-Energy Analysis. *Chem. Rev.* **2010,** *110*, 2005-2048.

(63) Siddiki, S. M. A. H.; Touchy, A. S.; Jamil, M. A. R.; Toyao, T.; Shimizu, K.-i. C-Methylation of Alcohols, Ketones, and Indoles with Methanol Using Heterogeneous Platinum Catalysts. *ACS Catal.* **2018,** *8*, 3091-3103.

(64) Segall, M. D.; Philip, J. D. L.; Probert, M. J.; Pickard, C. J.; Hasnip, P. J.; Clark, S. J.; Payne, M. C. First-Principles Simulation: Ideas, Illustrations and the CASTEP Code. *J. Phys. Condens. Matter* **2002,** *14*, 2717-2744.

(65) Vanderbilt, D. Soft Self-Consistent Pseudopotentials in a Generalized Eigenvalue Formalism. *Phys. Rev. B* **1990,** *41*, 7892-7895.

(66) Hammer, B.; Hansen, L. B.; Nørskov, J. K. Improved Adsorption Energetics within Density-Functional Theory using Revised Perdew-Burke-Ernzerhof Functionals. *Phys. Rev. B* **1999,** *59*, 7413-7421.

(67) Miyazaki, M.; Furukawa, S.; Komatsu, T. Regio- and Chemoselective Hydrogenation of Dienes to Monoenes Governed by a Well-Structured Bimetallic Surface. *J. Am. Chem. Soc.* **2017,** *139*, 18231-18239.

(68) White, R. J.; Luque, R.; Budarin, V. L.; Clark, J. H.; Macquarrie, D. J. Supported Metal Nanoparticles on Porous Materials. Methods and Applications. *Chem. Soc. Rev.* **2009,** *38*, 481-494.

(69) Zhang, B.; Asakura, H.; Zhang, J.; Zhang, J.; De, S.; Yan, N. Stabilizing a $Platinum_1$ Single-Atom Catalyst on Supported Phosphomolybdic Acid without Compromising Hydrogenation Activity. *Angew. Chem. Int. Ed.* **2016,** *55*, 8319-8323.

(70) Sun, Y.; Gray, S. K.; Peng, S. Surface Chemistry: A Non-Negligible Parameter in Determining Optical Properties of Small Colloidal Metal Nanoparticles. *Phys. Chem. Chem. Phys.* **2011,** *13*, 11814-11826.

(71) Hammer, B.; Norskov, J. K. Electronic Factors Determining the Reactivity of Metal Surfaces *Surf. Sci.* **1996,** *343*, 211-220.

(72) Nikolla, E.; Schwank, J.; Linic, S. Measuring and Relating the Electronic Structures of Nonmodel Supported Catalytic Materials to Their Performance. *J. Am. Chem. Soc.* **2009,** *131*, 2747-2754.

(73) Furukawa, S.; Ehara, K.; Ozawa, K.; Komatsu, T. A Study on the Hydrogen Activation Properties of Ni-Based Intermetallics: A Relationship between Reactivity and the Electronic State. *Phys. Chem. Chem. Phys.* **2014,** *16*, 19828-19831.

For Table of Contents use only

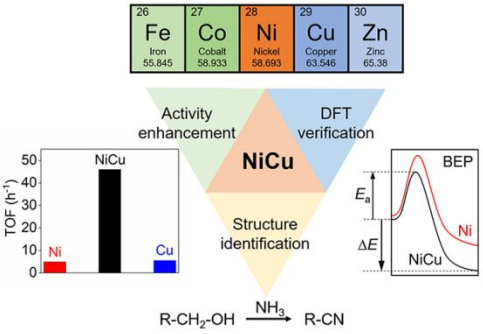

Identification of an Active NiCu Catalyst for Nitrile Synthesis from Alcohol

Yunzhu Wang[†], Shinya Furukawa*[‡§], and Ning Yan*[†]

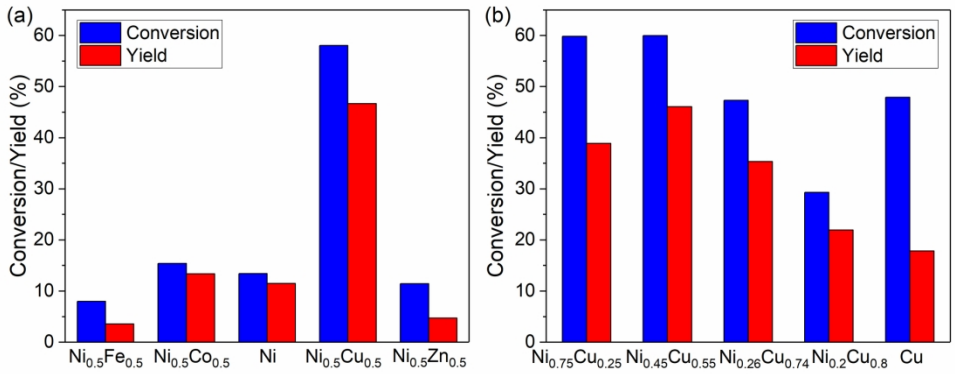

Figure 1. Catalytic activities of converting 1-butanol to butyronitrile with (a) various NiM/Al_2O_3 and Ni/Al_2O_3 catalysts prepared with DP method, and (b) various NiCu/Al_2O_3 and Cu/Al_2O_3 catalysts prepared with DP method. Reaction conditions: 1 μL/min 1-butanol, 8 mL/min NH_3, 20 mL/min N_2, 200 mg catalyst (or 60 mg $Ni_{0.2}Cu_{0.8}$), 160 °C, NH_3:1-butanol = 30:1.

179x79mm (300 x 300 DPI)

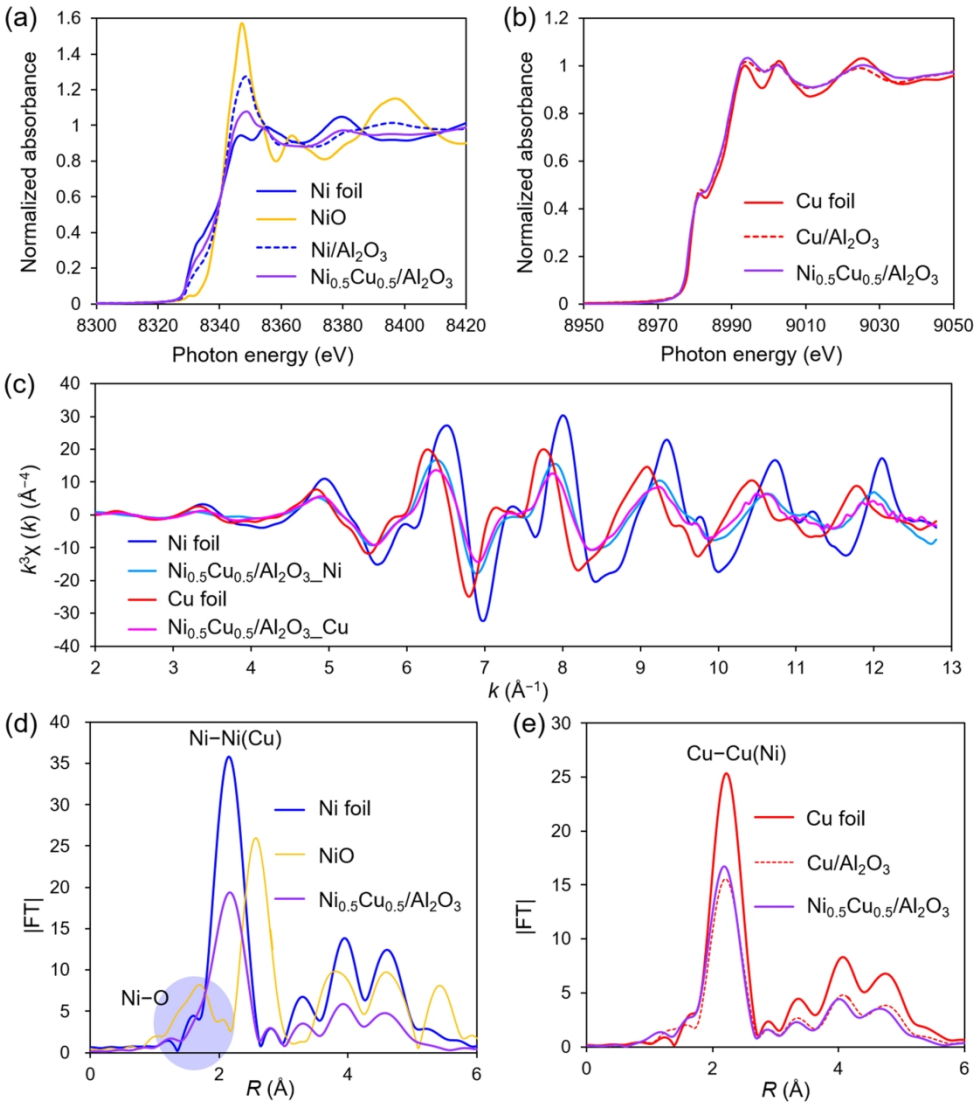

Figure 2. (a-b) XANES spectra, (c) EXAFS oscillations and (d-e) FT-EXAFS spectra of $Ni_{0.5}Cu_{0.5}/Al_2O_3$, Ni/Al_2O_3 and Cu/Al_2O_3 catalysts.

166x186mm (300 x 300 DPI)

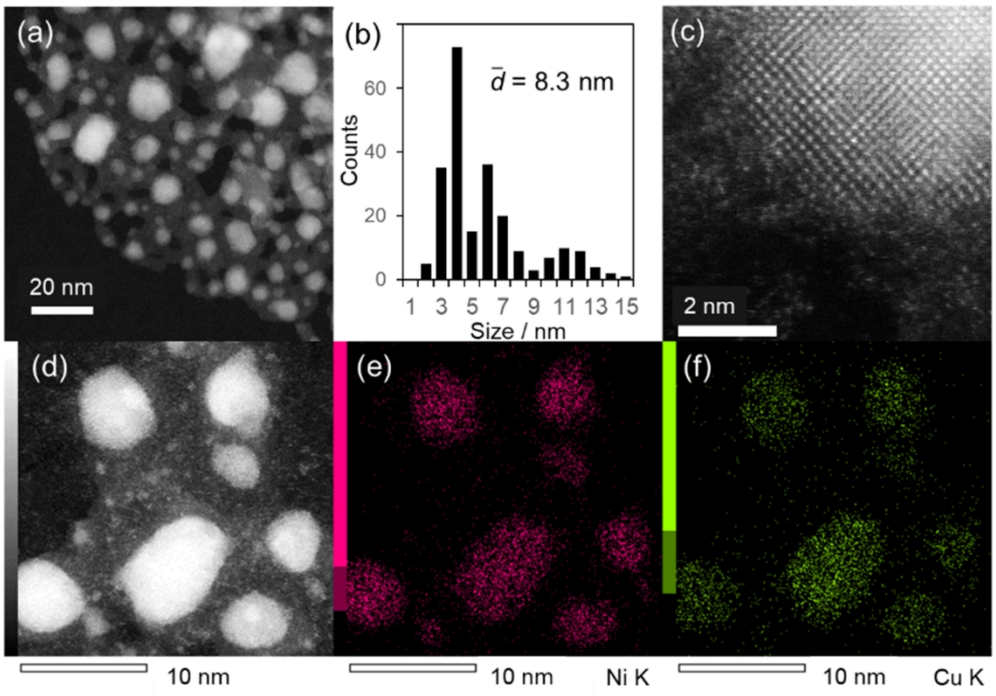

Figure 3. HAADF-STEM images of $Ni_{0.5}Cu_{0.5}$/ Al_2O_3 and the corresponding elemental maps of Ni and Cu acquired by EDS: (a) STEM image, (b) size distribution, (c) high-resolution image of an fcc crystal viewed along [100] direction, (d) close-up of some nanoparticles, and element sensitive maps of (e) Ni and (f) Cu.

160x112mm (300 x 300 DPI)

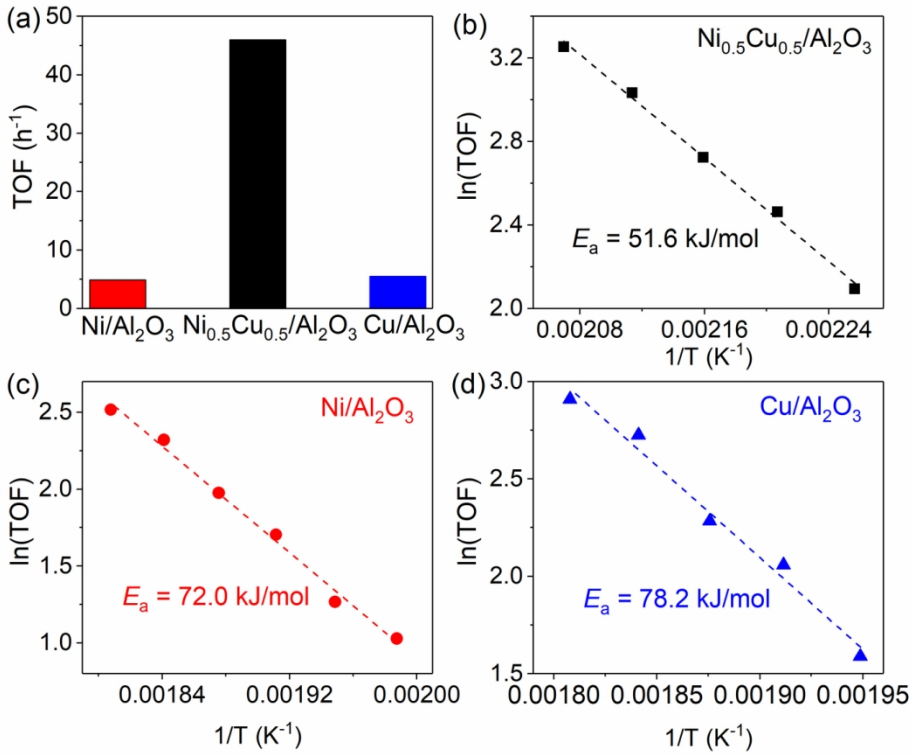

Figure 4. (a) TOFs towards production of butyronitrile at 210 °C. Reaction conditions: 4 ul/min 1-butanol, 8 ml/min NH_3, 92 ml/min N_2, 40 mg catalyst, 210 °C, NH_3:1-butanol = 7.5:1. (b-d) Activation energies of $Ni_{0.5}Cu_{0.5}/Al_2O_3$, Ni/Al_2O_3 and Cu/Al_2O_3 in the conversion of 1-butanol to butyronitrile. Reaction conditions: 1 ul/min 1-butanol, 8 ml/min NH_3, 92 ml/min N_2, 10 mg catalyst, NH_3:1-butanol = 30:1.

129x107mm (300 x 300 DPI)

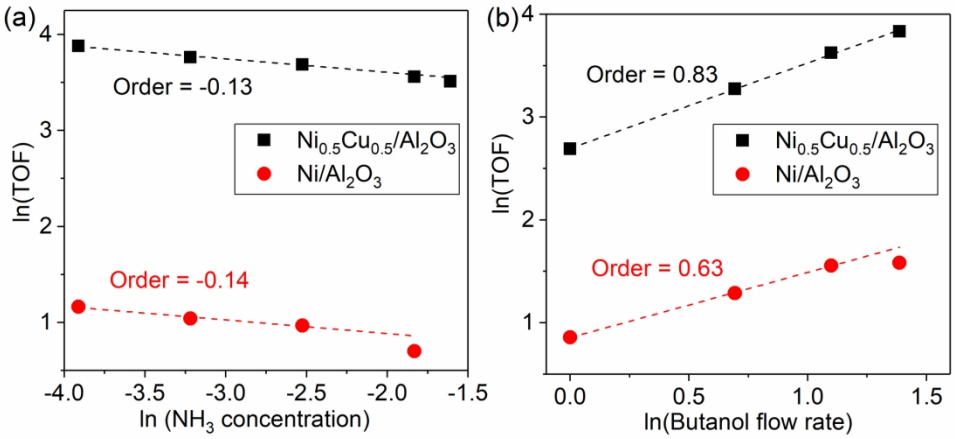

Figure 5. Plots of reaction orders for the conversion of 1-butanol to butyronitrile, of (a) NH_3, reaction conditions: 4 ul/min 1-butanol with 40 mg $Ni_{0.5}Cu_{0.5}/Al_2O_3$, or 3 ul/min 1-butanol with 80 mg Ni/Al_2O_3, 100 ml/min total gas flow rate with supplementing N_2, 210 °C; (b) 1-butanol, reaction conditions: 1 to 4 ul/min 1-butanol, 8 ml/min NH_3, 92 ml/min N_2, 40 mg $Ni_{0.5}Cu_{0.5}/Al_2O_3$ or 100 mg Ni/Al_2O_3, 210 °C.

179x95mm (300 x 300 DPI)

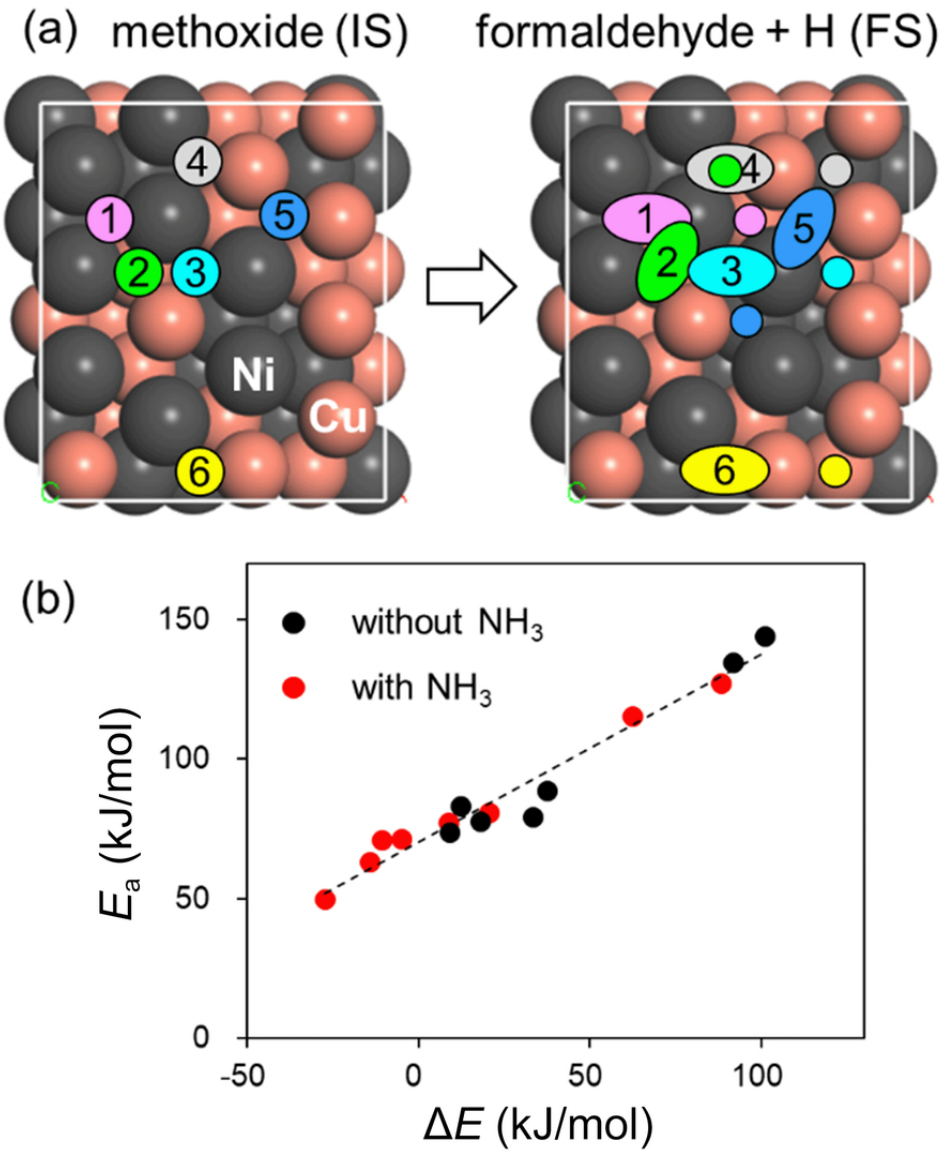

Figure 6. Adsorption conformation of methoxide and formaldehyde + H on $Ni_{0.5}Cu_{0.5}(111)$ alloy surface. Several conformations are numbered as NiCu-n. (b) Relationship between the calculated E_a and ΔE for Ni and NiCu in the absence and presence of ammonia.

77x94mm (300 x 300 DPI)

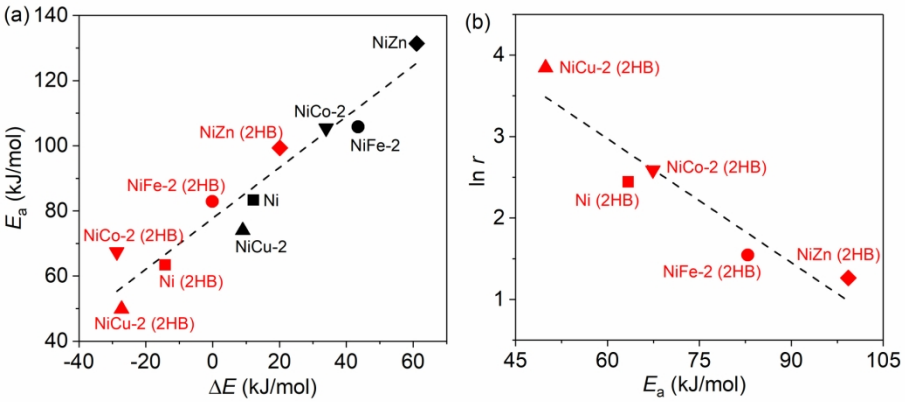

Figure 7. Correlations between (a) Ea and ΔE and (b) ln r (r: reaction rate = formation rate of nitrile) and Ea of C–H activation from methoxide to formaldehyde over Ni(111), NiM(111) (M = Fe, Co, and Cu) surfaces with NiM-2 configuration and intermetallic NiZn(101) surface. For (a), the plot was made among surfaces with ammonia co-adsorbed (red color) and without ammonia co-adsorbed (black color). For (b), the plot was made among surfaces with ammonia co-adsorbed.

179x79mm (300 x 300 DPI)

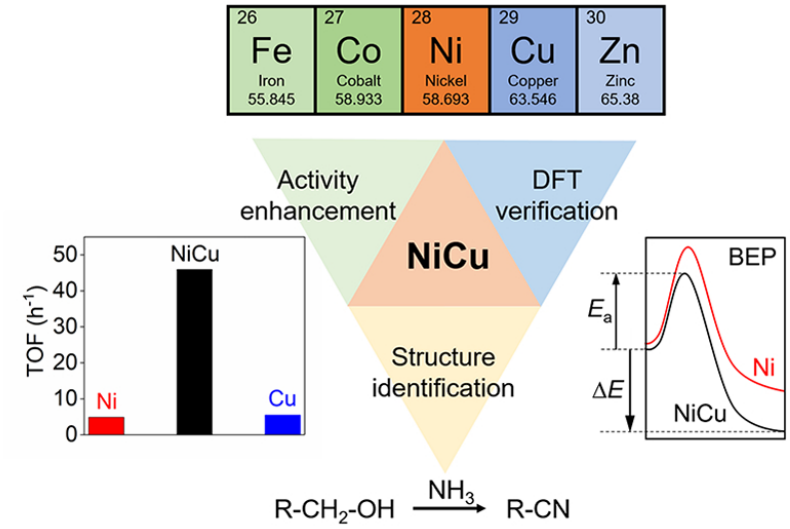
26
Fe
Iron
55.845
27
Co
Cobalt
58.933
28
Ni
Nickel
58.693
29
Cu
Copper
63.546
30
Zn
Zinc
65.38
Activity enhancement
DFT verification
NiCu
Structure identification
TOF (h-1)
50
40
30
20
10
0
NiCu
Ni
Cu
BEP
Ea
ΔE
Ni
NiCu
R-CH2-OH
NH3
R-CN